polymers

Article

Structural and Dynamical Properties of Polyethylene/Graphene Nanocomposites through Molecular Dynamics Simulations

Anastassia N. Rissanou [1,2,†,*], **Albert John Power** [1,3,†] **and Vagelis Harmandaris** [1,2,†,*]

[1] Institute of Applied and Computational Mathematics (IACM),
Foundation for Research and Technology Hellas (FORTH), Heraklion GR-71110,
Crete, Greece; E-Mail: ajpower@materials.uoc.gr

[2] Department of Mathematics and Applied Mathematics, University of Crete,
Heraklion GR-71409, Crete, Greece

[3] Department of Materials Science and Technology, University of Crete,
Heraklion GR-71003, Crete, Greece

[†] These authors contributed equally to this work.

[*] Authors to whom correspondence should be addressed; E-Mails: rissanou@iesl.forth.gr (A.N.R.);
harman@uoc.gr (V.H.); Tel.: +30-281-039-3746 (A.N.R); Fax: +30-281-039-3725 (V.H).

Academic Editor: Joong Hee Lee

Abstract: Detailed atomistic (united atoms) molecular dynamics simulations of several graphene based polymer (polyethylene, PE) nanocomposite systems have been performed. Systems with graphene sheets of different sizes have been simulated at the same graphene concentration (~3%). In addition, a periodic graphene layer ("infinite sheet") has been studied. Results concerning structural and dynamical properties of PE chains are presented for the various systems and compared to data from a corresponding bulk system. The final properties of the material are the result of a complex effect of the graphene's sheet size, mobility and fluctuations. A detailed investigation of density, structure and dynamics of the hybrid systems has been conducted. Particular emphasis has been given in spatial heterogeneities due to the PE/graphene interfaces, which were studied through a detailed analysis based on radial distances form the graphene's center-of-mass. Chain segmental dynamics is found to be slower, compared to the bulk one, at the PE/graphene interface by a factor of *5* to 10. Furthermore, an analysis on the graphene sheets characteristics is presented in terms of conformational properties (*i.e.*, wrinkling) and mobility.

1. Introduction

Graphene, an sp2-hybridized carbon layer of macroscopic dimensions but of atomic thickness, is a very important material with a wide range of novel applications due to its exceptional physical properties (*i.e.*, electron transport capacity, electrical conductivity, high intrinsic tensile strength and stiffness, high thermal conductivity) [1]. One of the most promising applications of this material is as a dispersed phase in polymer nanocompostites (PNCs), since even a very small concentration of graphene may dramatically affect the properties of the hybrid material [2–5]. Therefore, graphene based polymer nanocomposites have a very broad range of possible applications in many different areas [2,3]. For example, such hybrid materials can be used in electronic devices, for energy storage [3], while an emerging research direction is focused on biomedical applications [4].

Graphene based polymer nanocomposites are based on the incorporation of graphene in polymer matrices; thus the properties of the overall hybrid composite material depend strongly on how well graphene sheets are dispersed in the polymer. Furthermore, the improvement in the properties of the hybrid systems is influenced by the exfoliation techniques for the graphene flake as well as the dispersion method. An extensive review on different ways of exfoliation of graphite was given by Kim *et al*. [3], where advantages and disadvantages of each method were presented. The dispersion of graphene layers in the polymer matrix and possible functionalization of graphene sheets (e.g., graphite oxide) has been further recognized as crucial factors for the overall behavior (e.g., rheological, electrical, mechanical, thermal, and barrier properties) of nanocomposites [5].

Many simulation and experimental studies [1,6–19] explore the influence of the chemical functionalization of graphene on the various properties of the nanocomposites. For example, Konatham *et al*. [14] presented results based on atomistic Molecular Dynamics simulations combined with coarse grained Monte Carlo simulations, focused on graphene sheets dispersed in *n*-octane. They suggest that the functionalization of graphene sheets with short-branched hydrocarbons along the edges prevents agglomeration and leads to well-dispersed systems. They also mention the effect of the size of the graphene sheets, though their atomistic simulations are limited to rather small sheets. More recently Skoutzos *et al*. [15] presented results for syndiotactic poly(methyl methacrylate)/graphene nanocompostites, based on atomistic Molecular Dynamics simulations. They found that the introduction of oxygen-containing functional groups in graphene sheets leads to a great enhancement of the mechanical properties of the hybrid system, even at extremely low loading.

In addition to the previous discussion other factors, which can potentially influence the reinforcing capabilities on the various properties of the nanocomposites, are the *loading* of the graphene sheets (*i.e.*, their wt% in the polymer matrix), the *morphological characteristics* of the sheets (*i.e.*, wrinkles), as well as the *size* of the graphene sheets. Note, for example, that volume (or weight) fraction of the fillers in traditional polymer composites is much larger (e.g., ~60 vol%) compared to the typical one in graphene based polymer nanocomposites. For the latter, very low loadings (e.g., ~1–5 vol%) can cause

dramatic changes on various properties of the hybrid system. Ramanathan *et al.* [7], in a recent experimental work, have showed that the wrinkled single layer graphene and the functionalized graphene afford better interaction with the host polymer matrix and result to bigger enhancement of mechanical and thermal properties at exceptionally low loadings, compared to single-walled carbon nanotubes or expanded graphite. On the other hand, a multiscale simulation approach [16], based on a combination of molecular dynamics, molecular structural mechanics and finite element method, showed that the presence of ripples on the graphene flakes causes a decrease in the axial Young modulus of the nanocomposite, compared to the case of the flat graphene sheet. In this study a poly(methyl methacrylate) polymer matrix was used.

The work presented here is based on detailed atomistic Molecular Dynamics simulations of model PNCs systems and is focused on the effect of the size of the graphene sheets on various properties of the hybrid material. We are primarily interested in the way that *spatial heterogeneities*, due to the polymer/graphene interfaces, affect the *structural* and *dynamical behavior* of the entire system. Our goal is twofold. First, we study various properties of the graphene based PNC system at the molecular level and compare systems with graphene sheets of different sizes. Moreover, comparisons between these systems and a hybrid system with a periodic graphene sheet (a model of the "infinite" graphene sheet) are performed. Second, results concerning the translational and orientational dynamical behavior of the graphene sheet, as a function of its size, in the polymer matrix are presented. Furthermore, a conformational analysis for the sheet is performed.

This work is part of a more general detailed simulation study of polymer/graphene interfaces and graphene based polymer nanocomposites along multiple length and time scales. In our previous works, we have extensively studied the properties of various polymer/graphene interfaces through atomistic simulations in which infinite (periodic) graphene sheets were assumed [18,20,21]. The current work is focused on the properties of polyethylene/graphene nanocomposites with graphene sheets of various sizes. Here we have studied various PNC systems with the same concentration-loading of graphene (~3 wt%), where the host matrix is comprised of polyethylene (PE) chains. Note that, according to our knowledge, in all previous atomistic simulation studies of polymer/graphene systems rather small graphene sheets were modeled (e.g., up to 2 nm).

The rest of the paper is organized as follows: Section 2 contains information for the model, the simulation method and the analysis techniques that we have used. Our results, divided in subsections, concerning the polymer and the graphene properties are presented in Section 3, where a further division according to the presented property is performed. Finally the conclusions and the perspectives of the current work are presented in Section 4.

2. Models, Simulation Methodology and Analysis

Detailed atomistic molecular dynamics simulations for various polyethylene/graphene nanocomposites systems were performed. In more detail, we have investigated three PNCs systems with a single flexible graphene sheet of different size (S1, S2 and S3), as well as a periodic flexible graphene layer, which reflects a sheet of "infinite" size (SP). All systems were compared to a bulk polyethylene system (SB) and the deviations from the bulk behavior in the various properties were reported in [17,18]. More details for all systems are presented in Table 1.

Table 1. Details for the simulated systems: Name; Size of graphene sheet; Number of graphene atoms; Number of PE atoms.

Name	System	Graphene Atoms	PE Atoms
S1	(19×20) Å^2	190	5,456
S2	(49×51) Å^2	1,032	29,392
S3	(84×86) Å^2	2,546	72,688
SP	Infinite	2,432	18,480
SB	PE Bulk	-	9,240

Finite graphene sheets are modeled through an all-atom model, described by Bellido *et al.* [19], where partial charges are placed at all edge atoms. The concentration of graphene in the three systems with the finite-size graphene sheets is 3 wt% (weight percent), while for the periodic graphene the concentration is almost 10 wt%. For the representation of polyethylene a united atom model was used, where each methylene CH_2 and methyl CH_3 group was considered as a single Van der Waals interacting site. Polyethylene chains consist of 22 monomers.

Non-bonded interactions between polymer atoms, as well as between the carbons of graphene and the CH_2 (or CH_3) groups of PE chain, are described by a spherically truncated 6–12 Lennard–Jones potential of the form:

$$V_{LJ}(r_{ij}) = 4\varepsilon_{ij}\left(\left(\frac{\sigma_{ij}}{r_{ij}}\right)^{12} - \left(\frac{\sigma_{ij}}{r_{ij}}\right)^{6}\right), \quad r \leq R_c$$

where, the cutoff distance $R_c = 10$ Å. For intramolecular interactions 1–4 exclusions are made for PE and 1–3 for graphene. Tail corrections were applied to both energy and pressure. For the interactions between polyethylene and graphene atoms, the Lorentz–Berthelot rules were used (*i.e.*, arithmetic average for σ_{ij}: $\sigma_{ij} = \frac{1}{2}\left(\sigma_i + \sigma_j\right)$, and geometric average for ε_{ij}: $\varepsilon_{ij} = \sqrt{\varepsilon_i\varepsilon_j}$). A detailed description of the force field for both PE [22] and graphene [23] is presented in Tables A1 and A2 (in Appendix, at the end of the text); Table A1 contains the non-bonded parameters, while all bonded interactions are presented in Table A2.

Molecular Dynamics (MD) simulations were performed in the isothermal-isobaric (NPT) statistical ensemble, using the GROMACS package [24,25]. The pressure was kept constant using Berendsen barostat at $P = 1$ atm. The stochastic velocity rescaling thermostat was used to maintain the temperature at $T = 450$ K. The integration time step was 0.5 fs and periodic boundary conditions have been used in all three dimensions.

In order to obtain initial PE/graphene configurations finite graphene layers were placed at a close distance (about 0.5 nm) to a well-equilibrated polymer sample, taken from previous bulk PE simulations [18]. Graphene sheets were initially placed in the *xy*-plane at $z = 0$. All graphene atoms in the initial configuration were in the same plane (*i.e.*, there were no fluctuations in the sheet). During the simulation a complete decorrelation of a vector defined along the graphene layer is observed (for the finite graphene sheets), as it is discussed in more details in the Results section. In data analysis we exclude a certain number of configurations such as our results to be independent of the initial state. For the equilibration of the systems, first MD (Molecular Dynamics) simulations

for 50 ns were performed, during which the motion of the overall hybrid system was monitored. This time period is much larger than the time required for the de-correlation of PE end-to-end vector (about ~100 ps) [18]. Then production runs for times up to 100 ns were performed and several PE/graphene configurations were saved.

In a further step, all configurations that were gathered during the simulation runs were analyzed in a post processing procedure. Of particular importance are the *heterogeneous* characteristics of the hybrid systems, due to distribution of polymer/graphene intermolecular (adhesive) interactions. Therefore, properties of the polymer chains were examined as a function of the distance from the graphene sheets. Such an analysis for graphene-based polymer PNCs is in general not a trivial issue, due to the mobile, non-symmetric, polymer/graphene interfaces. The analysis presented here has been performed along radial distances from the center of mass of the graphene sheet, by creating spherical shells of increasing radius (*i.e.*, increasing distances form the graphene center). A sketch of this analysis scheme is depicted in Figure 1a. Because of the motion of the graphene sheet this calculation has to be repeated at every time step.

(a)   **(b)**
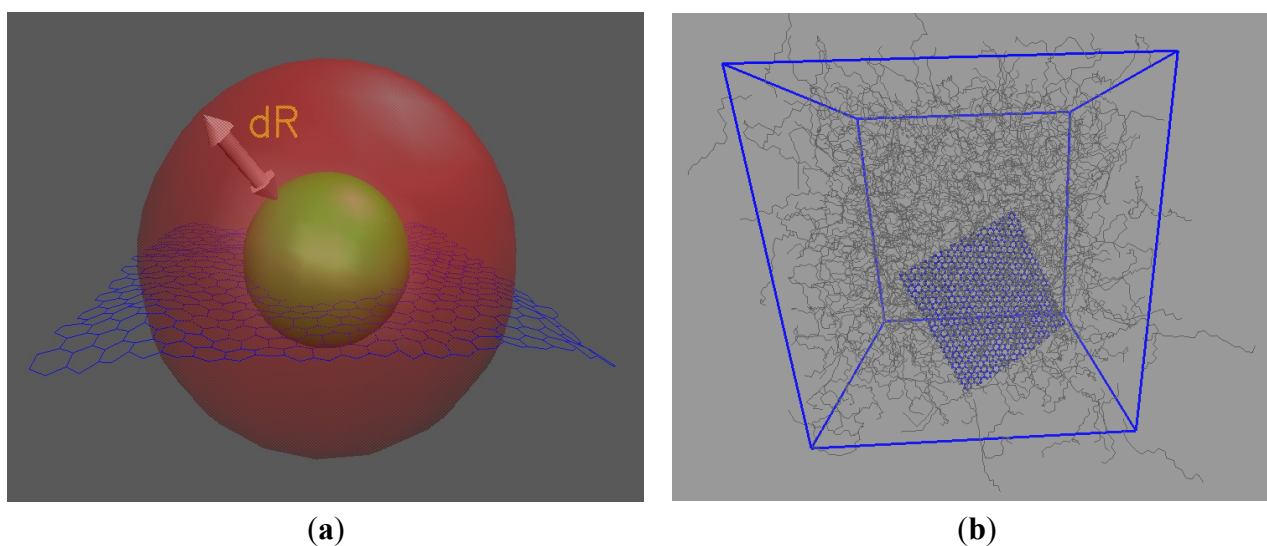
Figure 1. (**a**) A sketch of the analysis scheme in spherical shells; (**b**) A Snapshot of a model polyethylene/graphene system at 450 K. Graphene layer of size (49 × 51) Å^2. Additional videos from the simulations can be found in the supplementary material.

The mass density profiles were calculated according to the above-discussed radial distance, using spherical shells of thickness equal to 1 Å. The same binning was used for the calculation of the second rank bond order parameter. Thicker spherical shells were used for the calculation of dynamical properties, equal to 10 Å for both orientational and translational dynamics in the segmental level in order to improve statistics, whereas a 5 Å binning was used for the distribution of atoms according to their mean squared displacements in each shell. The choice of binning size (thickness of spherical shells) for the computation of each specific property is the result of an optimized balance between detailed information and improved statistics.

Furthermore, for the calculation of the density of PE as a function of the distance from the surface we applied the following procedure: The volume of each spherical shell is equal to:

$V_{shell} = \frac{4}{3}\pi\left[(r+dr)^3 - r^3\right]$, where r is the radius of a sphere, centered at the center of the graphene sheet and dr is the thickness of the shell. This volume contains both polymer and graphene atoms. In order to measure the precise PE density, we have to subtract the graphene volume from each spherical shell. For this purpose we calculated the mean density of graphene atoms within a sphere, around the center of the graphene sheet, with a radius equal to a distance, σ$_{CGR}$, of 3.47 Å (σ value for the C_{GR} atoms). Then the polymer number density is given by: $\rho_{PE} = \dfrac{N_{PE}}{\left[V_{shell} - \left(N_{GR}/\rho_{GR}\right)\right]}$, where N_{PE} and N_{GR} are the number of PE and graphene atoms, respectively, in the shell and $\rho_{GR} = \dfrac{N_{GR}}{\left(\frac{4}{3}\pi\sigma_{C_{GR}}^3\right)}$

from which the corresponding mass density is extracted.

We have also to underline here that this radial analysis has to be taken into account in the interpretation of the obtained results. In more detail, within a spherical shell, despite the fact that all atoms are equidistant from the center of graphene, there is a broad distribution of polymer atom/graphene atom distances, and a corresponding distribution of adhesive energies, which contribute differently to the calculated property. This effect is more pronounced for the intrinsic shells and attenuates as the radius becomes larger. However, the same would be the case if someone has used slabs (instead of spheres) as in the case of the analysis of polymer/solid interfaces with periodic-infinite solid surfaces. Only for the later system the parallel to the surface slabs is a natural way to calculate local properties due to the periodicity [18,20,21]. Below, for the infinite graphene sheet we compare polymer chain density profile through both ways of analysis. This issue is further discussed below.

3. Results and Discussion

Three different graphene sheets have been modeled (systems S1, S2, S3, see Table 1) as well as a PE system with a periodic ("infinite") graphene layer (SP) and a bulk PE system in the same conditions (temperature and pressure) in order to compare the properties of the PNCs with the unperturbed bulk one. A representative snapshot of a model system (S2) is shown in Figure 1b.

3.1. Polymer Properties

3.1.1. Density

We start the analysis of the model PNCs with the calculation of the mass monomer density profile of the polymer (PE) chains as a function of the distance from the graphene sheet. Average density profiles, which have been calculated for the center of mass of the monomers, $\rho(r)$, are presented in Figure 2a,d for all four systems. In Figure 2a, the polymer mass at each spherical shell has been divided with the total volume of the shell, which for the inner shells contains a number of graphene atoms as well, whereas the outer shells contain only polymer atoms. For this reason in Figure 2a PE mass density values at short distances are smaller than the corresponding bulk density value, while for longer distances bulk density is attained from the three systems with the finite graphene sheets. For the system with the infinite size graphene, monomer density approaches, but do not reach, the corresponding bulk value

since graphene mass exists in all spherical shells. In all four systems the density of PE close to the sheet is almost the same and unaffected by the size of the sheet. Away from the graphene layer, all curves reach/approach the bulk density value, though at different distances, as a result of the graphene sheet dimensions.
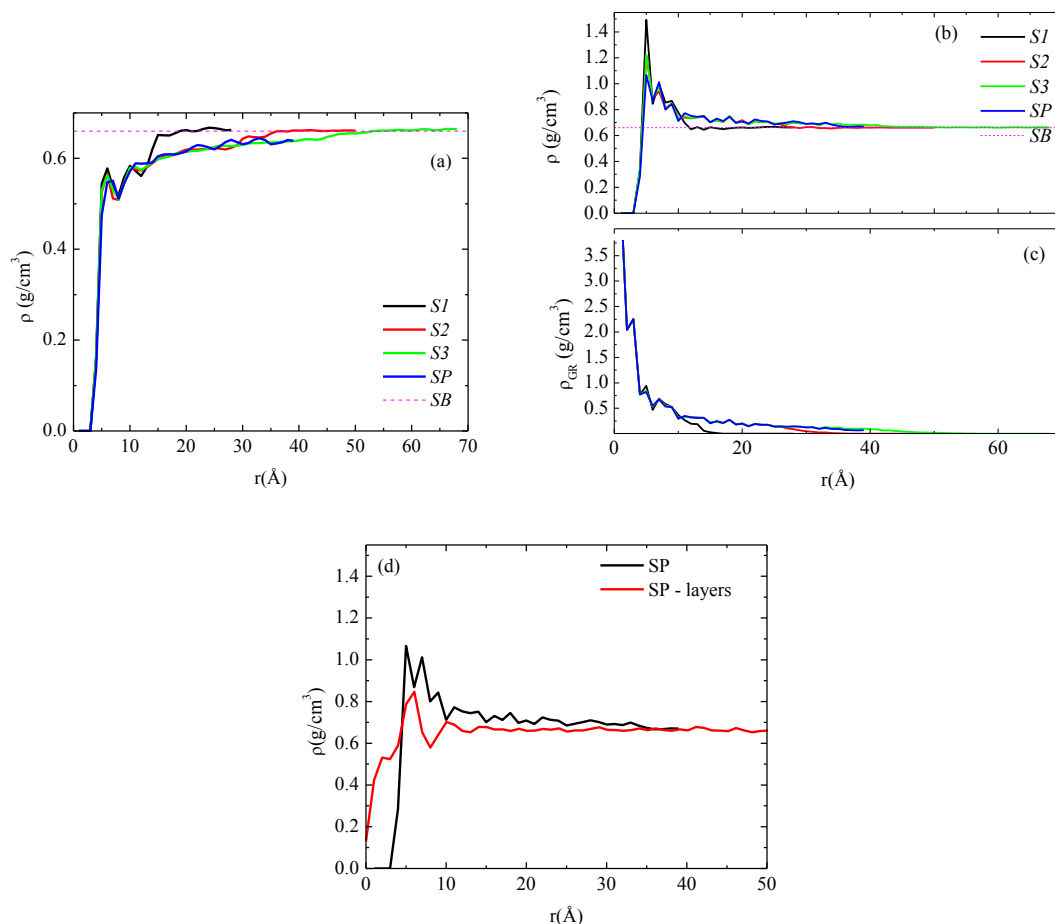
Figure 2. (**a**) Mass monomer density profiles of polyethylene as a function of *r* (distance from the center of the graphene layer) for the five systems studied here; (**b**) Density profiles of polyethylene chains excluding the volume occupied by graphene; (**c**) Mass density profiles of graphene layer as a function of *r*; (**d**) Density profile of polyethylene chains for the periodic graphene layer analyzed via spherical shells and parallel slabs.

In the next stage PE monomer density profiles are calculated dividing the polymer mass with a portion of the spherical shell volume that corresponds to this mass. For this purpose we have performed a rough estimation for the volume that graphene atoms occupy in each spherical shell and subtracted it from the total volume of the shell. This has been performed as mentioned in the previous section, through the following procedure: First, a sphere with a radius equal to a distance of 3.47 Å, which corresponds to the excluded volume between an atom in the graphene sheet and the polymer, is defined and the number of graphene atoms in this sphere is counted. No polymer atoms are included in this volume. Through these values the average effective volume occupied by each graphene atom in the graphene sheet is calculated. Second, the number of graphene atoms in any spherical shell is computed. Then, we calculate their effective volume within each spherical shell and subtract it from

the volume of the whole shell. Finally, polymer mass is divided with the remaining volume which corresponds to the polymer atoms. In Figure 2c the density of the amount of the graphene in each spherical shell is presented for all systems studied here. We observe that these curves attain the same values up to a specific distance, defined from the size of the sheet, beyond which no more graphene atoms are included in the spherical shell.

Chain density profiles, derived with the above procedure, for all model systems are shown in Figure 2b. All systems exhibit the same behavior: a peak of rather similar height (larger than the bulk value) is observed for all four systems at a distance/radius of about 0.5 nm, which denotes the attraction of the polymer from the graphene at short distances, while at longer distances the bulk density is attained.

As mentioned in Section 2 one issue related to the analysis method using spherical cells, is that this might not be the natural choice for systems with the infinite-periodic graphene sheet. For the latter the analysis in parallel slabs seems to be a more appropriate choice [18]. In Figure 2d we compare the density profiles of the polymer chains for this system (SP) and the two different analysis methods; *i.e.*, using spherical shells and parallel slabs. As we can see there are slight differences for the $\rho(r)$ data between the two methods in the region of 1–2 nm from the graphene sheet. Note finally that for the case of the parallel slabs the zero is defined on the position of the center of the graphene sheet, therefore due to thermal undulations of graphene it is probable to have polymer mass at zero distance.

In the following we analyze the distribution of ends and inner parts of the polymer chains at the PE/graphene interface. The preference of the chain ends to stay close to the surface, compared to the rest of the monomers, has been reported in previous studies of polymer/surface interfaces and it is primary of entropic origin [17]. We have also observed this behavior in our previous studies at the polymer/graphene interface of polymer thin films confined between two "infinite" (periodic) graphene sheets, as well as at polymer/vacuum interface [20,21,26]. A similar analysis has been performed in our current systems for both the end and the inner monomers. It is interesting to observe the effect of the motion of the sheet, the range of fluctuations and the different size on this tendency. In Figure 3a,b the density profiles based on the monomer center of mass for the end and the inner monomers are presented for all systems, respectively. The "end part" concerns only two monomers, the first and the last one, while the "inner part" is defined as the monomers of the chain in the interval $\left[\left(\dfrac{N}{2}-2\right), \left(\dfrac{N}{2}+2\right)\right]$, where N is the total number of monomers per chain. Following such a convention some monomers on the left and on the right side of the central part of the chain do not participate in the analysis; thus avoiding any contribution of the chain end effects in the analysis of the inner segments and vise-versa. For the infinite layer the preference of the ends for the interface is comparable to the one observed before for a PE/graphene system with a frozen graphene layer [17,21]; *i.e.*, thermal fluctuations of a very large ("infinite") graphene sheet are not very important for the overall chain arrangement at the PE/graphene interface.

Qualitatively different is the case for the systems with the finite graphene sheets. Data presented in Figure 3a for the two smaller sheets show that although an amount of end monomers are concentrated close to the graphene flake they do not exceed the highest density. In more details, for the S1 system the accumulation of end monomers in the bulk region is higher than the one at the interface, while for the S2 system the density of the end monomers at the interface increases and is almost equal to that in

the bulk region. For the largest sheet (S3 system) there is a small increase of the end monomers' density close to the graphene layer, compared to the two smaller systems (S1, S2), which roughly speaking indicates a tendency of the end monomers to be accumulated at the interface. The preference of the end monomers for the interface becomes clear only in the case of "infinite" graphene layer (SP). The density profiles for the inner monomers, shown in Figure 3b, have a complementary to the end monomers behavior, as expected. This is a combinatory effect of the size, the mobility and the fluctuations of the sheet and as it will be discussed in a following section, *i.e.*, the smaller the sheet the higher its mobility while the smaller its fluctuations. In addition, for the graphene sheets of finite size considerable system size effects exist, which are more pronounced for the smaller sizes.
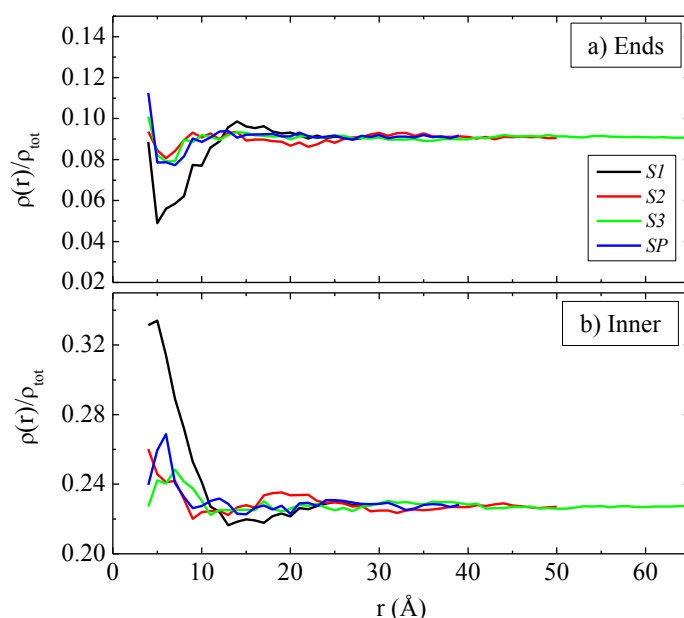
Figure 3. Mass monomer density profiles as a function of *R* (distance from the center of the graphene layer) based on (**a**) chain ends and (**b**) inner monomers of the polymer chain for the polymer/graphene nanocomposite systems.

3.1.2. *Conformational Properties*

We start the analysis of the chain conformations by calculating the average chain end-to-end distance, $R_{ee} = \left\langle R_{ee}^2 \right\rangle^{1/2}$, and the radius of gyration, $R_g = \left\langle R_g^2 \right\rangle^{1/2}$. An important question concerns whether chain swelling occurs due to chain adsorption at the polymer/graphene interface. In Table 2 we report data concerning the end-to-end distance of the polymer chains as a function of distance from the graphene sheets. As we can see chain dimensions are rather similar at all distances (and same to the bulk values) but the very first layer where a slight increase of the R_{ee} and R_g are observed. However, the latter values are within the error bars.

In the following we examine the orientation of the polymer chains close to the graphene layer in the segmental level through the v^{1-3} vector which connects two non-consecutive carbon atoms. In more detail, the second rank bond order parameter [27,28] defined as $P_2(\cos\theta) = \frac{3}{2}\left\langle \cos^2\theta \right\rangle - \frac{1}{2}$ is calculated. $P_2(\cos\theta)$ limiting values of −0.5, 0.0, and 1.0 correspond to perfectly parallel, random, and

perpendicular vector orientations relative to the graphene layer, respectively. In the above formula θ is the angle between the vector, which is defined along the molecule (here the v^{1-3} one) and the radial distance from the center of graphene. The bond order parameter of v^{1-3} for all four systems is depicted in Figure 4. In all cases there is an obvious tendency of the segments of the polymer chain for an almost parallel to the graphene layer orientation at short distances which is gradually randomized with the distance. However, there is a systematic increase of the order of the PE segments closest to the graphene layer with the increase of the size of the layers; the minimum values are about −0.17 for the two smaller sheets, whereas the value for the system with the largest sheet (S3) is about −0.25 very similar to that of the infinite sheet.

Table 2. Average chain end-to-end distance, $R_{ee} = \left\langle R_{ee}^2 \right\rangle^{1/2}$, and radius of gyration, $R_g = \left\langle R_g^2 \right\rangle^{1/2}$ for chains belonging in different adsorption layers, R. Corresponding bulk values: R_{ee} = 17.20 Å, R_g = 6.15 Å. Error bars are 3%–5% of the actual values based on block averaging techniques.

R (Å)	R_{ee} (Å)				R_g (Å)			
	S1	S2	S3	SP	S1	S2	S3	SP
0–6	17.30	17.46	17.48	17.48	6.44	6.55	6.51	6.46
6–10	17.28	17.41	17.44	17.46	6.32	6.54	6.50	6.45
10–20	17.24	17.33	17.36	17.41	6.28	6.31	6.36	6.35
20–30	17.23	17.28	17.32	17.37	6.21	6.24	6.28	6.27
30–40	17.22	17.25	17.30	17.35	6.18	6.22	6.23	6.26
40–50	-	17.24	17.27	17.33	-	6.20	6.23	6.23
50–60	-	17.24	17.25	17.31	-	6.18	6.21	6.19
60–70	-	-	17.25	-	-	-	6.20	-
70–80	-	-	17.25	-	-	-	6.19	-
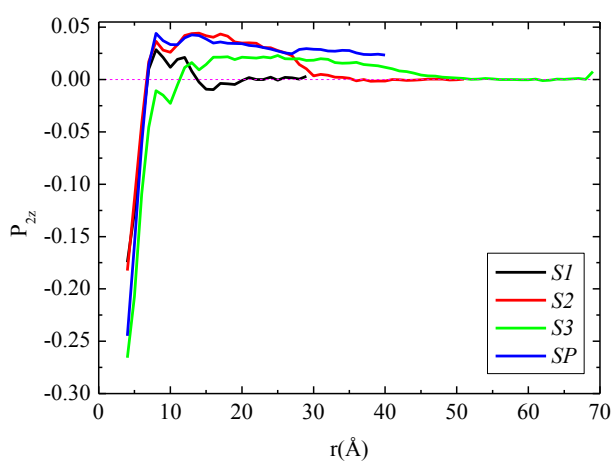
Figure 4. Second rank bond order parameter $P_2(\cos\theta)$ of polyethylene for v^{1-3} vector as a function of R distance (distance from the center of the graphene layer) for all polymer/graphene nanocomposite systems studied here.

A further analysis of the PE chain conformations is based on the calculation of the distribution of the torsional (dihedral) angles, P_{dih}, in different distances from graphene. This is of particular

importance since for PE the distribution of its (backbone) dihedral angle is critical for the determination of its overall chain conformation (e.g., radius of gyration and characteristic ratio). In the analysis performed here all torsional angles with values between −60° and +60°, are defined as "trans", whereas outside this interval angles are considered as "gauche+" or "gauche−". Our results which are depicted in Figure 5a–c indicate clear spatial heterogeneous dihedral angle distribution, for all PNCs. Figure 5a contains a comparison of the distribution of the torsional angles in the (spherical) first adsorption layer (*i.e.*, from 0 to 6 Å) for the four systems together with the corresponding bulk system. A non-negligible enhancement of the trans states with a consequent reduction of the gauche ones is observed for all systems compared to the bulk case. This observation reflects the more ordered PE chains close to the graphene sheet, something which has been reported previously as well, for thin polymer films supported by graphene or graphite [17,18]. Enhancement of "trans" population would be expected to affect the cystallinity of PE chains as well as the mechanical properties of the hybrid PNC system. This will be studied in a forthcoming work. Moreover no differentiation in the torsional angle distributions among the various sizes of graphene sheets is detected. The corresponding information for the most distant adsorption layer (*i.e.*, bulk region) is presented in Figure 5b, where the curves are completely identical to each other and to the corresponding bulk one.
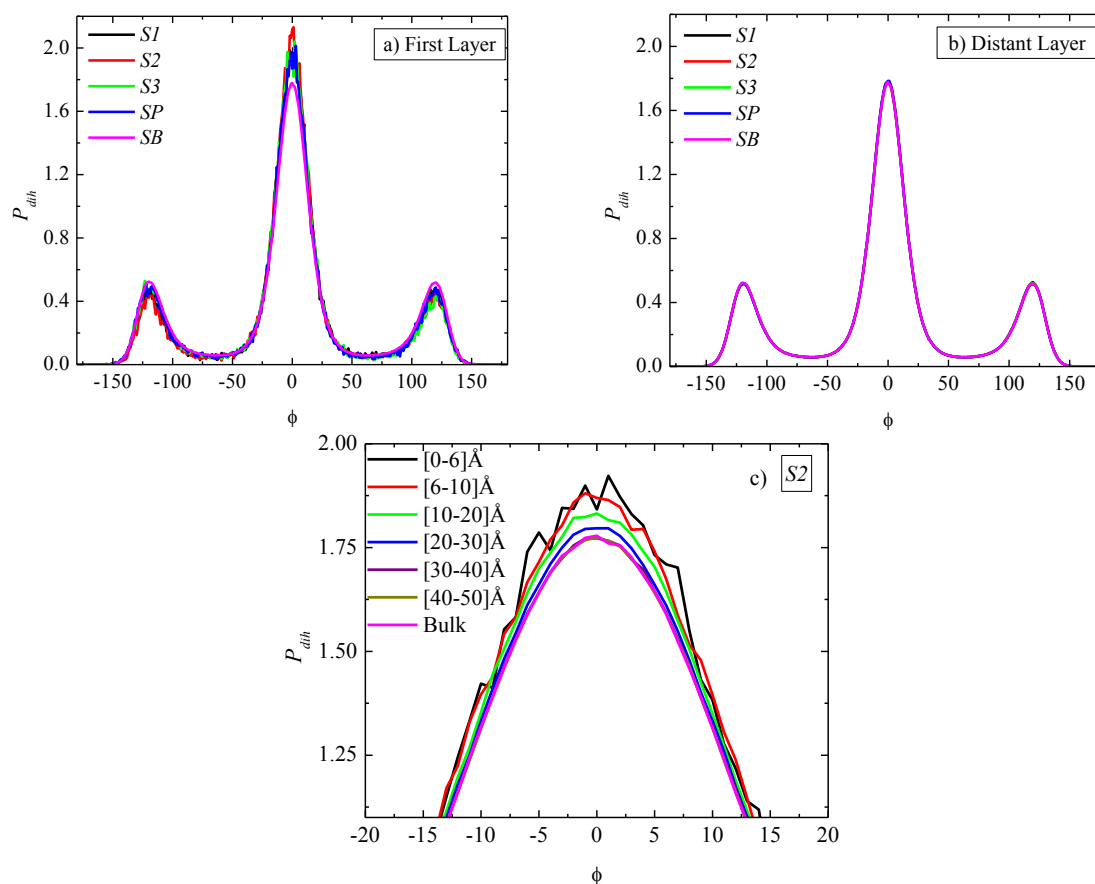
Figure 5. Torsional angles distribution as a function of *R* distance (distance from the center of the graphene layer). (**a**) Data for the first adsorption layer (*R* = 0.6 nm) for all systems; (**b**) Data for the last adsorption layer (distant layer) (*R* = *L*BOX/2) for all systems; (**c**) Magnification for all spherical shells of the (S2) system. In all cases the corresponding bulk curve is included.

Furthermore, if we compare P_{dih} as a function of radial distance from the center of the graphene sheet, the enhancement of "trans" states remains, presenting a small but gradual decrease compared to the first adsorption layer, up to a different distance depending on the system. Beyond a specific distance for each system the rest of the curves coincide with those of Figure 5b. The enhancement of "trans" states for dihedral angles of the S2 system, and for the various regimes studied here, is presented in Figure 5c, where it is clear that the curves are distance dependent, despite the rather noisy data due to the small size of each regime. Overall, the distance above which all P_{dih}'s become similar to the bulk P_{dih} defines the width of the interphase for the particular property and the way that it is affected by each graphene sheet. The effect can be thought as a combination of the differentiations among the sheets (*i.e.*, size, mobility, fluctuations), which will be analyzed in detail in a following section.

Based on the above discussion of the spatial chain structural-conformational heterogeneities, a rough estimation of the distance beyond which the bulk behavior of the hybrid PNC system, is attained can be given as: ($\sim r \leq 10$ Å), for the smallest graphene sheet, (S1), extended to larger values ($\sim r \leq 30$ Å) for the S2 system and even further ($\sim r \leq 40$ Å) for the S3 system, while for the infinite graphene layer (SP) system size limitations do not allow the prediction of a specific value for the distance beyond which the bulk behavior is attained.

3.1.3. Dynamics

We continue the analysis of the model PNCs by presenting dynamical properties of PE as a function of the distance from the graphene layer. Using the time autocorrelation function (ACF) of the second Legendre polynomial: $P_2(t) = \frac{3}{2}\langle \cos^2 \theta(t) \rangle - \frac{1}{2}$, we first study the *orientational* dynamics at the segmental level. The v^{1-3} vector, which has been defined previously, is used and $\theta(t)$ is the angle of this vector at time t relative to its position at $t = 0$. Results for the autocorrelation function, $P_2(t)$ are presented in Figure 6a–c for all hybrid PE/graphene nanocomposites studied here. Corresponding data for a bulk PE system are shown in these Figures as well. Note that for these calculations we monitor the position of each segment/vector only for the time period it belongs to the corresponding analysis regime.

First, in Figure 6a data concerning the $P_2(t)$ function of PE chains, averaged throughout the entire hybrid systems, are presented for the four nanocomposite systems as well as for the bulk PE system. There are only small differences between the different systems, *i.e.*, hybrid systems show a slightly slower average segmental dynamics compared to the bulk one. In more detail, at very short times $P_2(t)$ curve that corresponds to the system with the smallest graphene sheet (S1) coincides with the bulk one, while for the other three systems $P_2(t)$ curves attain higher values. This can be thought as a result of the fast motion of the very small sheet, which hinders the immediate effect on the polymer chains, so for a very short period they behave like being in bulk, but they diverge rapidly from this behavior.

Second, in Figure 6b $P_2(t)$ at different radial adsorption layers (*i.e.*, different distances from the graphene sheet's center) for the S1 system are shown. PE chains in the first adsorption layer show much slower segmental dynamics compared to the bulk one. A faster decorrelation is then observed moving away from the surface up to a specific distance, while beyond this all curves coincide. This distance determines the width of the PE/graphene interphase for the orientational segmental

dynamics. Qualitatively similar data were found also for the other two hybrid PE/graphene systems (S2, S3). An extended interphase is also detected here as a result of the different kinetic behavior among the graphene flakes of various sizes. The width of the interphase is found to be rather similar to the one reported previously, concerning the distribution of the dihedrals angles.
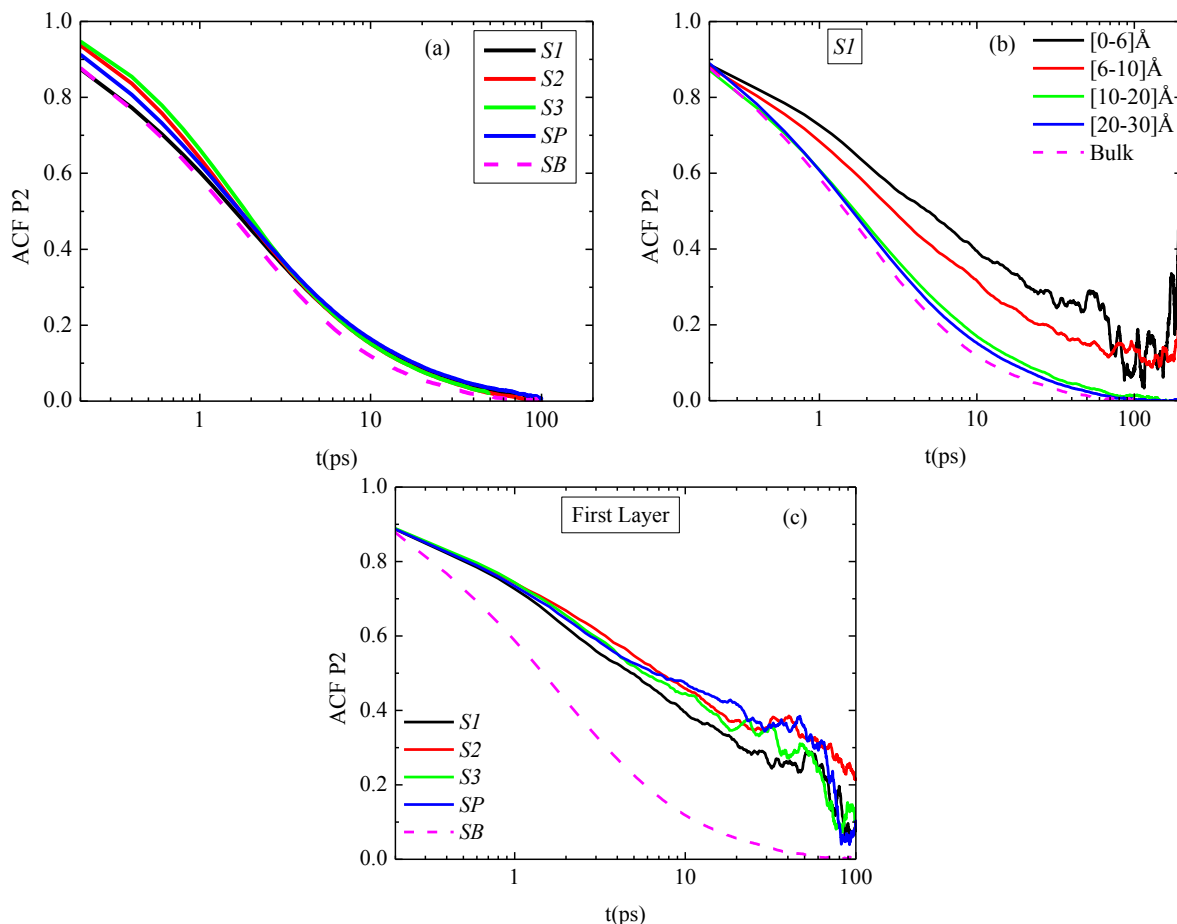
Figure 6. Time autocorrelation function (ACF) of bond order parameter $P_2(t)$ as a function of time for the characteristic vector v^{1-3} of polyethylene for all systems. (**a**) Average $P_2(t)$ values are over the entire system; (**b**) $P_2(t)$ values for the S1 system, for various spherical shells; (**c**) $P_2(t)$ values for all systems in the first adsorption layer. In all cases the corresponding bulk system is presented as well.

To further quantify differences, concerning the segmental dynamics of the PE chains in the vicinity of the PE/graphene interface, $P_2(t)$ for the first adsorption layer for all systems studied here are shown in Figure 6c. It is clear that the relaxation of PE chains is much slower in all systems compared to the bulk case. In addition, there are small differences between the different systems; the S1 system exhibits slightly faster relaxation (larger mobility) compared to the S2 and S3 systems. Overall, in agreement to the structural characteristics of the hybrid systems, it seems that the behavior of the PE chains for the two larger systems is closer to the infinite one, whereas for the smallest system the differences are more pronounced.

Another important aspect concerns the examination of the polymer chain dynamics at the polymer/graphene interface of the PNC, compared to previous studies of PE/graphene thin films [18,20,21].

Slight differences exist between the current study and our previous publications concerning PE/graphene systems (using a periodic and frozen graphene layer). In more detail data reported here show a slightly faster decorrelation of the $P_2(t)$ function of v^{1-3} vectors that are at the polymer/graphene interface (distances up to about 1 nm) compared to the frozen graphene sheets, whereas for longer distances relaxation times are identical for both cases. The analysis in the last studies was based on layers parallel to the graphene sheet and equidistant from the surface. For this reason we observed that at long distances the $P_2(t)$ curves overlap with the corresponding bulk curve. It is the periodicity of the sheet that favors this geometry in contrast to the present work where the finite size of the sheets demands a different geometric scheme for the analysis of the model configurations.

The effect of the PE/graphene interface on the PE segmental dynamics of each system can be further quantified by computing the corresponding segmental relaxation times, through proper fits of curves shown above (Figure 6a–c), with a Kohlrausch–Williams–Watts (KWW) stretch exponential function [29] of the form: $P_2(t) = A \exp\left[-\left(\dfrac{t}{\tau_{KWW}} \right)^\beta \right]$, where, A is a pre-exponential factor which takes into account relaxation processes at very short times (e.g., bond vibrations and angle librations), τ_{KWW} is the KWW relaxation time and β the stretch exponent, which describes the broadness of the distribution of the relaxation times (*i.e.*, the deviation from the ideal Debye behavior—$\beta = 1$). Then, segmental relaxation time, τ_{seg}, is calculated as the integral of the KWW curves through:

$$\tau_{seg} = \frac{\tau_{KWW}}{\beta} \Gamma\left(\frac{1}{\beta} \right)$$ where $\Gamma()$ is the gamma function.

The results of the above analysis for both the segmental relaxation time τ_{seg} and the β exponent for PE chains of the S2 system are presented in Figure 7a,b, respectively. Bulk values are also shown in this figure with dashed lines. It is clear the much slower orientational dynamics (larger segmental relaxation time τ_{seg}) of PE chains that are very close to the graphene layer (about 0.5 nm); τ_{seg} is about 10 times larger than the bulk one. As expected polymer segments become more mobile as their distance from the graphene layer increases, reaching a plateau, bulk-like regime, at distances of about 4.0–5.0 nm away from the graphene sheet. In addition, β-exponent values of PE chains at all distances are smaller than the bulk value (~0.62), shown in Figure 7b with dashed line.

Qualitatively similar to the above behavior is also the case for the other systems studied here. In order to compare the behavior of the PE chains closest to the graphene layer we present in Table 3 the τ_{seg} and the β exponent for the different systems in the first adsorption layer as well as for the bulk system. We observe that as the size of the graphene layer increases the relaxation time of the PE chains slightly increases, *i.e.*, their mobility becomes slower, for the cases of the finite graphene sheets. However, in periodic graphene a slightly smaller relaxation time, compared to the finite sheets, is observed, which can be attributed to the reduced motion of the periodic graphene's center-of-mass. Values for the β exponent are similar for all systems (around 0.4), smaller than the bulk value of 0.62. The latter indicates a *broader* distribution of the polymer segmental dynamics, compared to the bulk one, even for distances far away from the graphene sheets, where the *average* τ_{seg} is similar to its bulk value. Therefore, when the way that polymer/graphene interfaces affect the dynamical properties of a PNC system is considered, average properties do not provide the full information, but rather the whole distribution of segmental dynamics should be examined. This results shows that dynamical heterogeneities

present in polymer nanocomposites systems is an even more complex phenomenon than those appeared in polymer/solid interfacial systems (e.g., PE confined between graphene sheets [18]), for which the behavior far away from the surface reaches the bulk one.
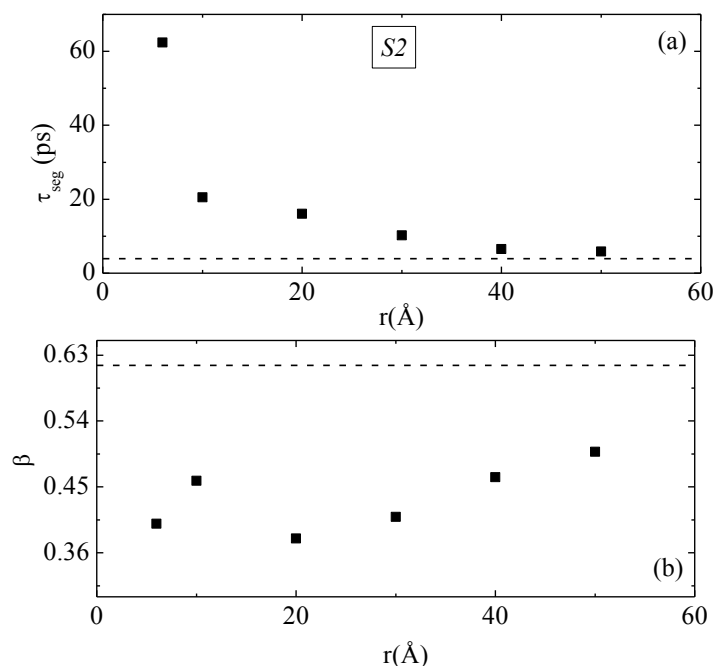
Figure 7. (**a**) Segmental relaxation time, τ_{seg}, of v^{1-3} characteristic vector based on $P_2(t)$ time autocorrelation as a function of R (distance from the center of the graphene layer) for the S2 system; (**b**) The stretch exponent β, as extracted from the fit with KWW functions. Dashed lines represent τ_{seg} and β values of bulk PE under similar conditions ($T = 450$ K, $P = 1$ atm).

Table 3. Average segmental relaxation times τ_{seg} and stretch exponents β of PE chains for all systems studied here (columns 2 and 3). τ_{seg} values and stretch exponents β for all systems in the first adsorption layer are shown in columns 4 and 5. Error bars are obtained using block averaging techniques.

| Systems	τ_{seg}-Average (ps)	β-Average	τ_{seg}-1st Layer (ps)	β-1st Layer
S1	4.6 ± 0.3	0.53 ± 0.05	44 ± 6	0.40 ± 0.05
S2	6.7 ± 0.4	0.46 ± 0.05	62 ± 6	0.40 ± 0.05
S3	6.1 ± 0.4	0.49 ± 0.05	63 ± 6	0.38 ± 0.05
SP	5.8 ± 0.4	0.52 ± 0.05	47 ± 5	0.41 ± 0.05
SB	3.9 ± 0.3	0.61 ± 0.05	-	-

In the next stage, we examine the *translational* segmental dynamics of PE chains. To distinguish translational dynamics for different layers we have calculated the average segmental mean-square displacement (msd) defined as:

$$g^j(\tau) = \left\langle \left[\mathbf{r}_i(t+\tau) - \mathbf{r}_i(t) \right]^2 \right\rangle$$

where j is a specific radial region, i is a particular segment (CH$_2$ or CH$_3$ group here) within region j, $r_i(t)$ and $r_i(t + \tau)$ are the coordinate vectors of segment i at time t and $t + \tau$, respectively, whereas

brackets $<>$ denotes statistical average. Note, that in the analysis used here a segment i contributes to the above average msd for a given time interval τ and for a radial region j, if and only if it was constantly present in that region in the entire course of time τ. First, in Figure 8a data concerning $g^j(\tau)$ for all (radial) adsorption layers for the S2 system are shown. The segmental dynamics of the polymer atoms that are closer to the graphene sheet atoms (mainly in the first two adsorption layers) is slower compared to the one of the atoms in the other layers. On the contrast, segments belonging to the other regimes, (above second layer) exhibit rather similar dynamics, which is slightly slower to the bulk one, shown in Figure 8a with dash line.

In Figure 8b data concerning $g^j(\tau)$ for the first adsorption layer ($j = 1$) for all systems studied here are presented. It is clear that the segmental dynamics of the PE chains closest to the graphene layers is slower, compared to the bulk one, for all model PNCs systems. In addition, there is a slight dependence of the PE segments $g^j(\tau)$ msd on the size of the graphene sheet mainly in the ~5–20 ps time regime, *i.e.*, the segmental dynamics for the small-graphene system (S1) is faster than the two other systems, whereas $g^j(\tau)$ for the biggest graphene system (S3) is similar to the periodic-infinite case. In Figure 8c $g^j(\tau)$ msd data for PE chains belonging in a radial layer far away from the graphene sheet are shown for all systems. Segmental translational mobilities of different systems are very similar to each other, slightly slower than the unconstrained bulk one.
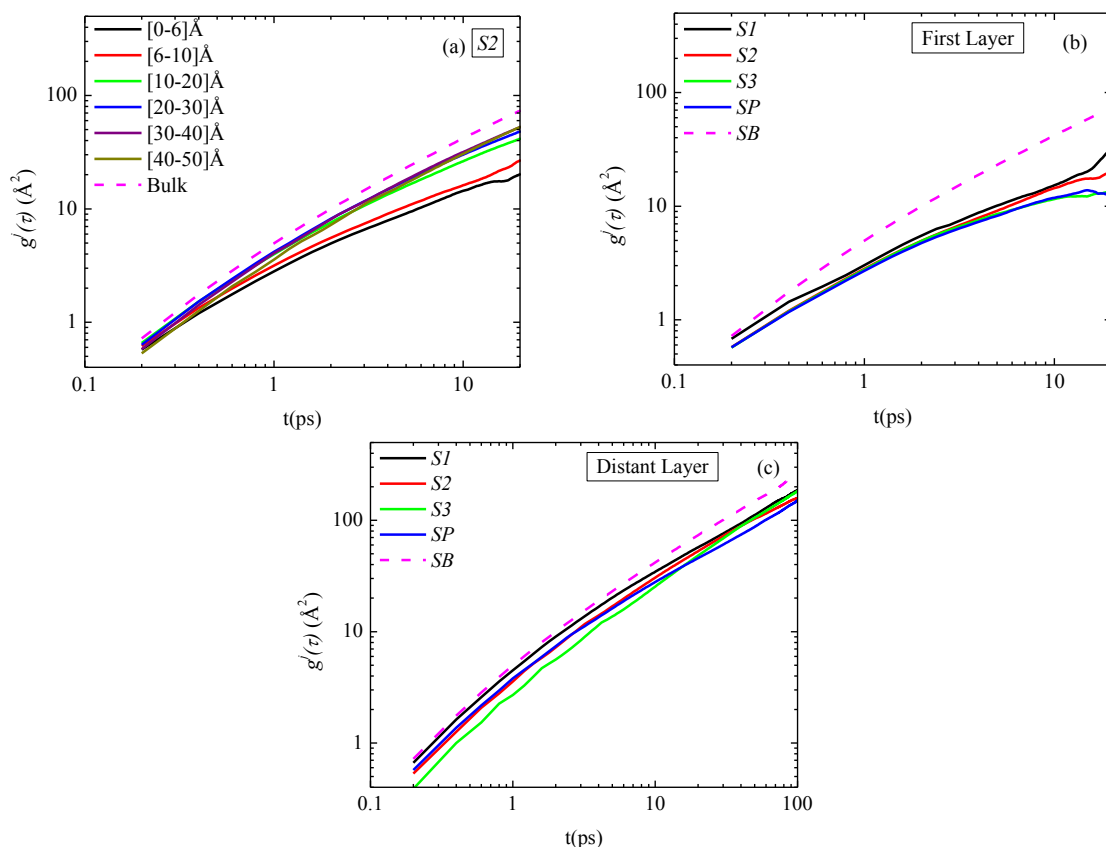
Figure 8. (**a**) Segmental mean squared displacement for polyethylene chains along *R* (distance from the center of the graphene layer); (**a**) Values for the S2 system, for various spherical shells; (**b**) Data for the first adsorption layer (distant layer) (*R* = 0.6 nm) for all systems; (**c**) Data for the last adsorption layer (*R* = *L$_{BOX}$*/2) for all systems. In all cases the corresponding bulk curves are included.

The *dynamical heterogeneity* of polymer atoms discussed above can be examined in greater detail if we consider the probability distribution of segmental $g^j(\tau)$ msds for a specific time period τ. An important aspect is related to the disturbance of such a distribution, compared to the bulk polymer system. Data for the distribution of $g^j(\tau)$ for the S2 system and a specific time period similar to the bulk segmental relaxation time ($\tau = 5$ ps) are shown as bars in Figure 9a–c for three different radial regimes: 0–6 Å, 20–25 Å and 45–50 Å. In all cases the distribution of a bulk system is shown with a solid line. First, a broad distribution is shown for all regimes, especially for the second and third regime shown here (Figure 9b,c), for which msds have been found in the range 0–80 Å^2 similar to the one of the bulk system. Segments in the first regime (atoms closest to the graphene sheet) show a more narrow distribution, with msds in a 0–40 Å^2 range. Second, the probability distribution of $g^j(\tau)$ msd's, of atoms belonging in the first adsorption regime (Figure 9a), is larger than the bulk one for small displacements (Δr^2), up to about 10 Å^2. On the contrary, the probability to find larger msds, above about 10 Å^2 is smaller than the bulk one. As we move far away from the graphene sheet the probability distribution of the $g^j(\tau)$ msd's data approaches the bulk one, *i.e.*, probability of finding small msds decreases, whereas the probability to find larger msds increases. This is particular clear for the longer distances 45–50 Å, which exhibit very similar distribution to the bulk PE atoms.
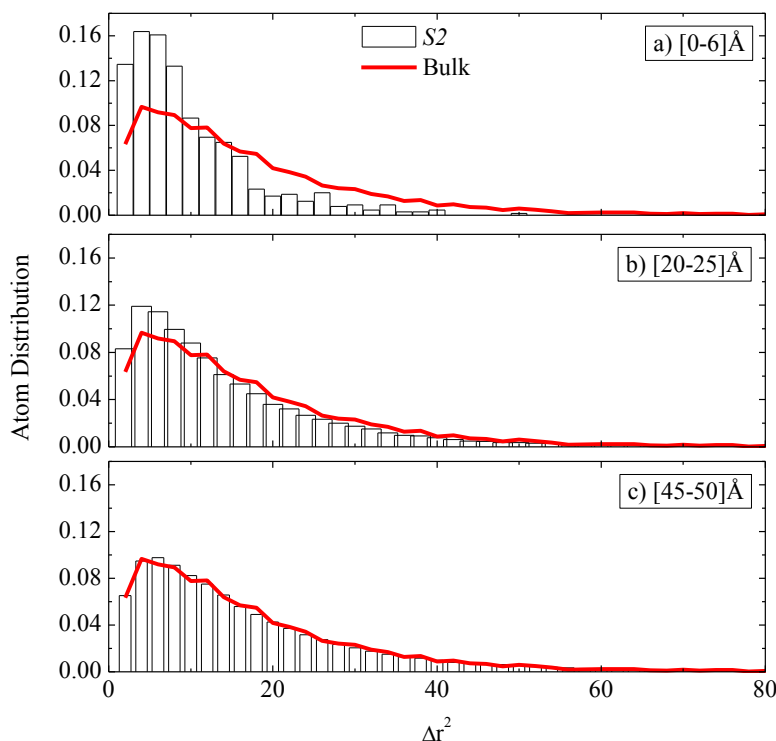
Figure 9. Probability distribution of the mean squared displacements, $g^j(\tau)$, for the S2 system at a specific time period ($\tau = 5$ ps) for three different radial regimes: (**a**) 0–6 Å; (**b**) 20–25 Å and (**c**) 45–50 Å. In all cases the distribution of a bulk system is shown with a solid line.

Data concerning the probability distribution of $g^j(\tau)$, computed at three different regimes and for the specific time period discussed above ($\tau = 5$ ps), are shown in Figure 10a–c for all S1, S2 and S3 systems, respectively. All systems exhibit a similar behavior to the S2 system discussed above (see

Figure 9); *i.e.*, for segments belonging to the radial regime closest to the graphene surface there is a larger probability for smaller msds, compared to the bulk one. This is in agreement with the average $g^j(\tau)$ data presented above in Figure 8a–c. On the contrary, segments belonging to the regime that is far away from the graphene sheet show similar distribution to the bulk system. In the same graph the distribution for the infinite-periodic system (SP) is shown as well. The latter exhibit qualitatively similar behavior as expected. There is only a small difference in the far distant layer for the SP system that still exhibits larger (smaller) probabilities for small (large) distances, compared to the bulk one. The reason for this difference is that due to the "infinite" size of the periodic graphene layer there are always some atoms in the radial analysis used here that are in small distances from the graphene atoms. The msds of these atoms is on the average smaller; thus increasing the probability to find smaller msds in the graphs shown in Figure 10c.
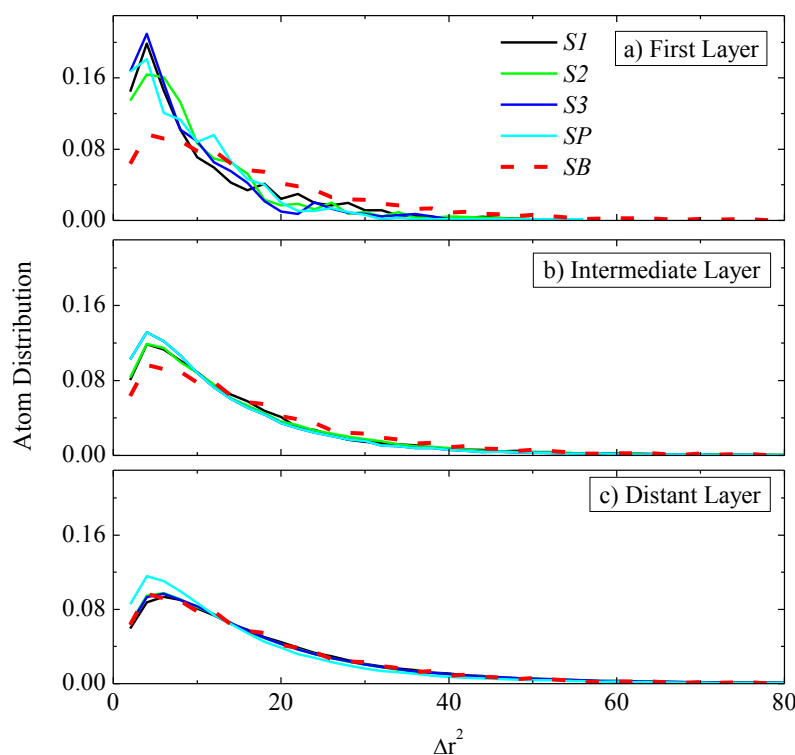

Figure 10. Probability distribution of the mean squared displacements, $g^j(\tau)$, for all three systems at a specific time period (τ = 5 ps) for three different regimes: (**a**) First layer: 0–6 Å; (**b**) intermediate layer: (10–15 Å for S1, 20–25 Å for S2, 30–35 Å for S3, 15–20 Å for SP) and (**c**) distant layer: (25–30 Å for S1, 45–50 Å for S2, 65–70 Å for S3, 35–40 Å for SP). In all cases the distribution of a bulk system is shown.

3.1.4. Desorption Kinetics

An important quantity related to the response of the nanocomposites to external stimuli (e.g., changes in temperature or imposed deformations) is the adsorption/desorption behavior of polymer atoms at the polymer/graphene interface. The latter is examined by calculating the rate with which atoms, which are initially close to the graphene sheet, are desorbed from this regime with time. In more detail, we label atoms that are initially (at time t_0) within the adsorption (radial) regime defined

in the range 0–1.5 nm, and then we compute the number of atoms that are still in the same regime after time t, $n(t_0 + t)$. In Figure 11a the percentage of the adsorbed atoms, $n(t_0 + t)/n(t_0)$ is shown. To improve statistics model configurations were analyzed every few hundreds of ps (different t_0 values were considered using multiple time origin technique).

All systems shown in Figure 11a exhibit the same behavior: Atoms are desorbed from the graphene sheet with a stretched exponential-like behavior and all of them are desorbed from the graphene flakes in time periods of about 100 ps. To further quantify the kinetic behavior of PNCs all data shown in Figure 11 were fitted with a KWW equation. Then a characteristic relaxation time, τ_{des}, was calculated from the integral of the KWW curves. $\tau_{des} = 36.5 \pm 0.5\,\mathrm{ps}$ has been computed for the three PNC systems (S1, S2 and S3) and a value of $\beta = 0.57 \pm 0.05$ for the β-exponent. The broad distribution of the PE atom desorption kinetics provides another indication of the strong dynamic heterogeneities appeared the PNCs due to the polymer/graphene interfaces.
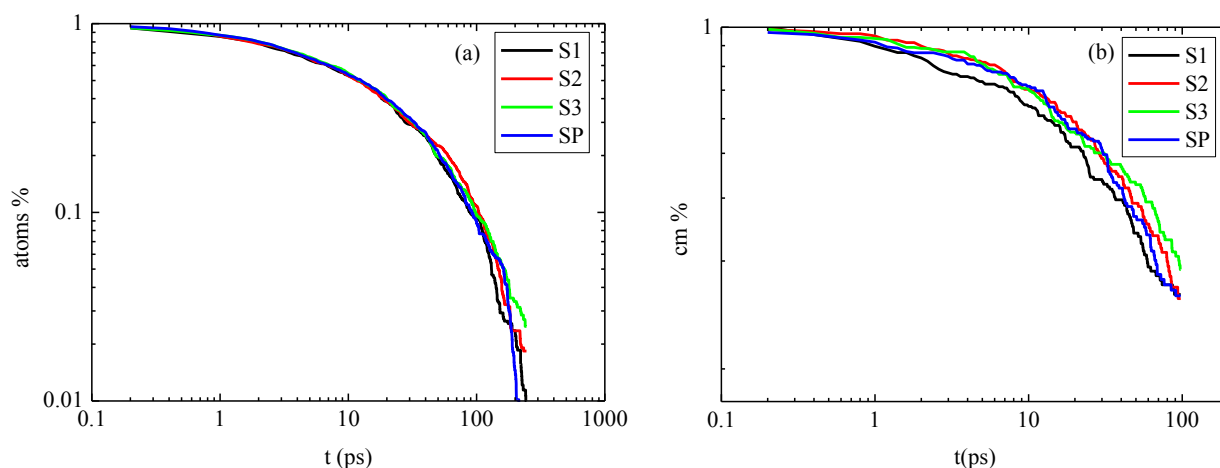
Figure 11. Evolution of the percentage of (**a**) polymer atoms and (**b**) chain center-of-masses that are within the adsorption regime, as a function of time for all systems.

The same calculation was made for the desorption kinetics of the whole chains based on their center of masses (cms) as depicted in Figure 11b. The decay of the percentage of the adsorbed cms in the range 0–1.5 nm as a function of time has a similar behavior to the one of atoms, though desorption kinetics is slower in this case, as expected. A fit with a KWW function provides the corresponding values for the desorption of the PE cms: $\tau_{des} = 52.07 \pm 1.0$ ps and $\beta = 0.66 \pm 0.05$.

3.2. Graphene Properties

Translational Dynamics: In this section results concerning the properties of the graphene flakes, in the hybrid model polymer-graphene systems studied here, are presented. First, the dynamical behavior of the graphene sheet in each system is examined by computing its center-of-mass mean squared displacement: $\Delta R_G^2 = \left\langle \left(R_G(t) - R_G(0) \right)^2 \right\rangle$, where $R_G(0)$ and $R_G(t)$ are the positions of the center of mass of the sheet at time 0 and t, respectively. Data for ΔR_G^2 as a function of time for the three finite systems are presented in Figure 12. Note that the center-of-mass of the "infinite" graphene sheet does not exhibit any translational or orientational motion as expected. Several important observations are

made in Figure 12. First, all graphene sheets exhibit a considerable translational motion; *i.e.*, they are moving along distances of about 20–100 nm for the time period of the current simulations (50 ns), much larger than their size. Second, the smaller the graphene sheet the higher its mobility. More specifically in Figure 12 a big difference in the mobility is found between the smallest sheet (S1) and the other two sheets (S2, S3). For the S2 and S3 systems, mean squared displacements attain comparable values though the smaller one (S2) is again a little faster. Third, all curves are rather noisy due to poor statistics. This is not surprising if we consider the small graphene percentage (~3 wt%) in all systems.

In order to check whether the diffusion of the graphene sheets in the polymer matrix is linear we present in the sub-plot of Figure 12 an effective time-dependent diffusion coefficient for graphene defined as: $D(t) = \Delta R_G^2 / (6t)$ as a function of inverse time. For a system exhibiting linear (Fickian) diffusion a plateau-time independent value is expected for long time, that is the macroscopic diffusion coefficient. It is not possible to find such a time regime here, especially for the two larger graphene sheets, showing that the systems practically do not yet follow linear diffusion. For the smaller system there is a short linear-like time period from 15 to 20 ns where D is about 0.07 Å²/ps.
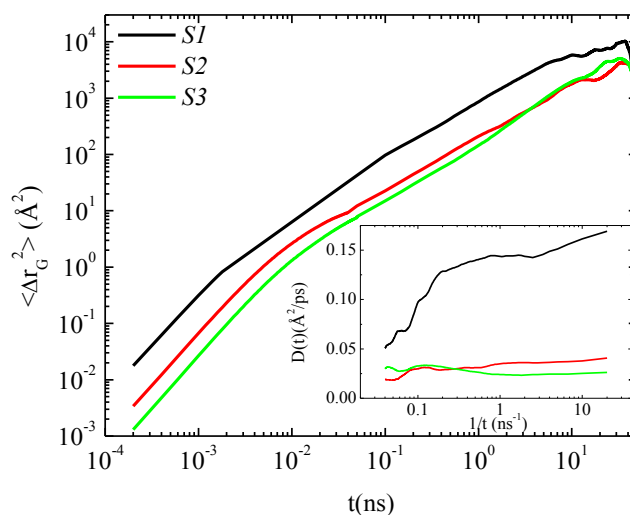
Figure 12. Mean squared displacement as function of time for the center of mass of the graphene sheet for the S1, S3 and S3 systems. Inset graph: Effective time dependent diffusion coefficient of graphene sheets as a function of inverse time for the three systems.

Orientational Dynamics: Next we study the dynamical behavior of the graphene sheets related to their orientational motion. This can be quantified through the de-correlation of a vector along the graphene sheet. In more detail, we have calculated the first bond order parameter $P_1(t) = \langle \cos\theta(t) \rangle$, where $\theta(t)$ is the angle of the vector under consideration at time t relative to its position at $t = 0$. The $P_1(t)$ time autocorellation function as a function of time is presented in Figure 13 for the three hybrid systems. The vector which has been chosen for this calculation is the one connecting the center of the graphene sheet with a corner atom (*i.e.*, half diagonal), denoted in Figure 14a with a dash line. A complete decorrelation of $P_1(t)$ is observed for all systems during the simulation time but at different characteristic time scales; the smaller graphene layer (system S1) decorrelates within 1 ns, much faster than the other two, which decorrelate within 10–20 ns.

To further quantify the orientational dynamics of the graphene sheets we calculate corresponding relaxation times based on fittings of $P_1(t)$ data with KWW functions [29]. Results for the orientational relaxation time ($\tau_{graphene}$) and the β exponent are presented in Table 4. For the smallest sheet (S1) segmental relaxation time is about one order of magnitude smaller than the other two systems whereas the largest sheet (S3) has an almost double $\tau_{graphene}$ compared to the S2 system. Moreover β values indicate very narrow distribution of relaxation times in all cases (*i.e.*, β ~0.9–1.0). Note that as expected a similar behavior is observed for any other vector chosen along the graphene, mainly in long time regime, above 100 ps, which is dominated by the overall orientational motion of the whole graphene sheet.
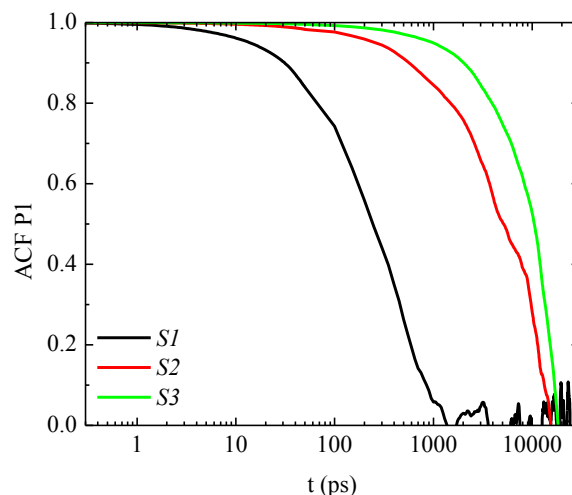

Figure 13. The time autocorrelation function of bond order parameter $P_1(t)$ as a function of time for a characteristic vector along the half diagonal of the graphene sheet for S1, S2 and S3 systems.

Table 4. Orientational relaxation times $\tau_{graphene}$ defined for a characteristic vector along the half diagonal of the graphene sheet and stretch exponents β for S1, S2 and S3 systems. Error bars are obtained from the standard deviations, based on block averaging calculations throughout the simulation runs.

Systems	$\tau_{graphene}$ (ps)	β
S1	360 ± 20	0.90 ± 0.04
S2	8,300 ± 450	0.88 ± 0.04
S3	15,300 ± 800	0.96 ± 0.04

Wrinkling of Graphene: The final part of the analysis of the graphene sheets concerns their conformational characteristics in terms of fluctuations—wrinkling behavior. For this purpose we define one cross line on the sheet (denoted with red full line in Figure 14a), parallel to the *y*-direction, and observe its motion during the simulation starting from a completely straight line (*i.e.*, a planar conformation of the graphene sheet). The line passes from a series of graphene atoms, which are spaced one lattice constant apart in a sequential way. Initially, when the flake is planar, all these atoms are on a straight line and in the following their vertical shift is recorded with respect to the plane of the sheet at its instantaneous position. This requires an Eulerian transformation of the coordinates from the original Cartesian system to a new one defined by: (a) the first atom of the straight line (zero point)

and (b) three vectors, the first two of which are defined along the plane of the graphene sheet at its current position, the third being the one normal to the plane of the first two, as it is represented schematically in Figure 14b.

(a)   (b)

(c)
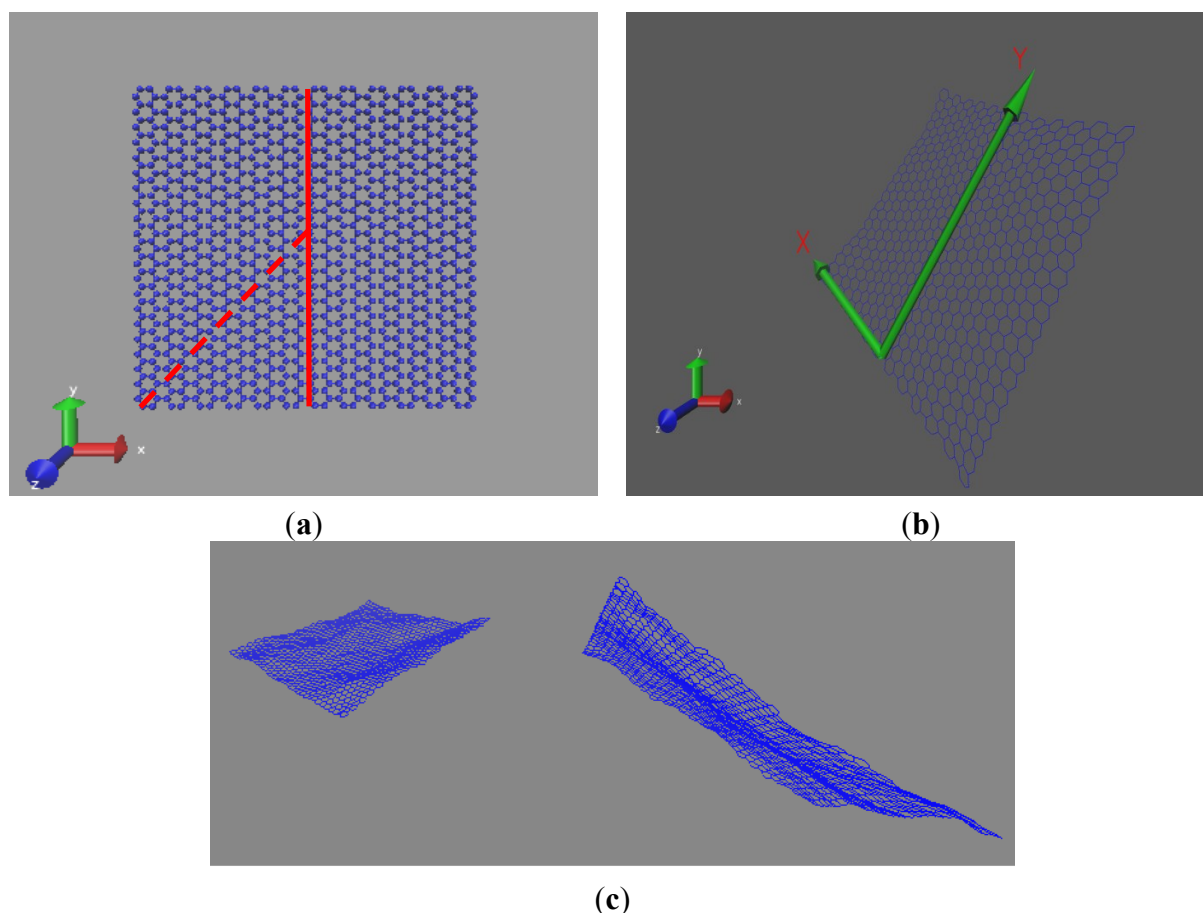
Figure 14. (**a**) A schematic representation for the conformational analysis of graphene sheets. The characteristic vector along the half diagonal is shown; (**b**) A schematic representation for the Eulerian transformation of the coordinates from the original Cartesian system to a new one at the instantaneous position of the sheet; (**c**) A characteristic snapshot of graphene layers with fluctuations.

A "wavy" motion is observed with crests and troughs for all systems studied here. This is a combinatory result of thermal fluctuations as well as fluctuations imposed by the (attractive) energetic interactions between the graphene and the polymer matrix. However, this motion does not happen in a periodic way, even for the largest graphene sheet studied, but it seems more like random thermal fluctuations. Two representative snapshots are depicted in Figure 14c. The motion of the defined line at different times is presented for the S2 sheet in Figure 15, where we have chosen four time points together with the initial snapshot ($t = 0$). This is only a qualitative picture in which various shapes of the line are observed. It is interesting to see that there are cases where only crests or only troughs are detected and cases where crests and troughs exist in the same line. For the latter cases a difference in the number of crests and troughs along the line among the four systems is expected due to the different size of the sheets. Wrinkling of graphene has been studied experimentally by transmission electron microscopy measurements on individual graphene sheets in vacuum or air [30]. These measurements

detected out-of-plane deformations of the sheets of the order of 1 nm. On top of that atomistic Monte Carlo simulations which were performed on single-layer graphene [31] in vacuum, found ripples spontaneously appeared on graphene sheets with a size distribution peaked around 80 Å, are in agreement with the experimental findings.
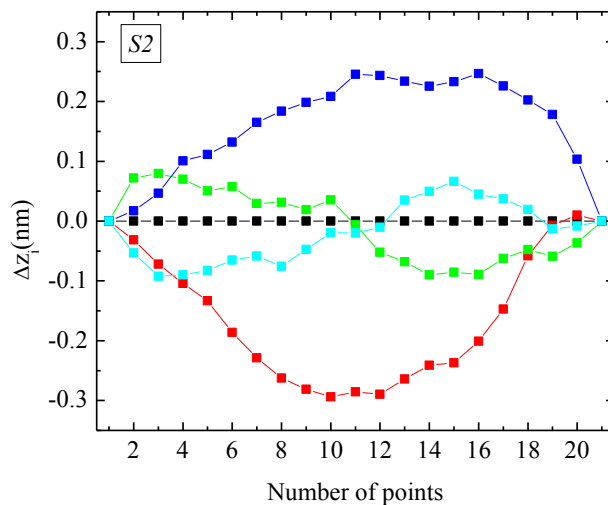
Figure 15. The out of plane motion of the cross line defined on the graphene sheet for all the atoms of the line at four different time spots (colored symbols), together with the initial snapshot (black symbols, $t = 0$) for the S2 system.

A rough quantification of the above pictures in order to perform a comparison among the systems is based on the calculation of the square root of the second moment of the out-of-plane displacement, averaged over all the atoms of the line, $\sqrt{\left\langle \Delta z_i^2 \right\rangle}$, throughout the simulation. Results for all systems are presented in Table 5. Increasing amplitude of fluctuations is observed as the size of the graphene sheets become bigger. Nevertheless the statistics of these calculations is poor and as a consequence the error bars are very large. For the accurate estimation of such long-time fluctuations longer simulations are required. A further investigation of the wrinkling on graphene sheets, concerning a more detailed analysis of graphene conformations, as well as the frequency of the interchange among different conformations (*i.e.*, from one crest to one trough or to crests and troughs) will be the subject of a following study.

Table 5. The square root of the second moment of the out of plane graphene motion averaged over all the atoms of the cross line for S1, S2 and S3 systems.

Systems	S1	S2	S3
$(<\Delta z^2>)^{0.5}$ (Å)	0.035 ± 0.023	0.058 ± 0.060	0.085 ± 0.083

4. Conclusions

The overall behavior of graphene based PNCs is strongly affected by the spatial heterogeneities induced by the presence of polymer/graphene interfaces. In the present work we have presented results from a detailed atomistic simulation study of various graphene based polymer (polyethylene)

nanocomposites. The simulation method was carried out by following a hierarchical modeling strategy consisting of: (a) generation of initial structure; (b) equilibration of the hybrid system for long time; (c) execution of long MD simulations (production runs) for times up to 100 ns; and (d) a detailed analysis of the atomistic configurations gathered in part (c). Here such a detailed analysis was proposed based on averaging over atoms (or chains) within radial layers equidistant from the center of the graphene sheet. PNCs with graphene sheets of different sizes but with the same concentration of graphene (~3 wt%) were modeled in order to study the *effect of the graphene size* on the properties of the hybrid material.

The above-discussed detailed analysis allows us to examine the way *spatial heterogeneities* are related to structural and dynamical features of the hybrid PNC system as a function of distance from the polymer/graphene interface. Results can be summarized as follows:

(a) Local *structural* and *conformational* features were analyzed at the level of both individual segments (atoms or bonds) and entire chains. The local monomer PE mass density near the graphene plane exhibits a maximum due to the intermolecular PE/graphene (adhesive) interaction, which is similar for all systems. Chain segments show a tendency for an almost parallel to the graphene layer orientation at short distances which is gradually randomized as one moves away from the interface, over a distance roughly equal to (~3–5 nm). However, there is a systematic increase of the order of the PE segments closest to the graphene layer with the increase of the size of the layers. In addition, increase of "trans" population in the dihedral angle distribution at the PE/graphene interface compared to the bulk one has been observed, which reflects the more ordered polymer chain structures.

(b) *Orientational* relaxation of PE chains in the hybrid PNC systems at the segmental level was quantified through the time autocorrelation function of the second Legendre polynomial. Qualitatively similar behavior was found for all systems: PE chains closest to the graphene sheet show much slower segmental dynamics (segmental relaxation time τ_{seg} is about 10 times larger) compared to the bulk one. Faster $P_2(t)$ decorrelation is observed moving away from the interface up to a specific distance (about 4–5 nm), while beyond this, all curves coincide. A slight dependence of chains mobility on the size of the graphene layers was also found; the larger the sheet, the slower the segmental dynamics of the PE chains. In addition, broader distribution of the polymer segmental dynamics, compared to the bulk one was found (smaller β-exponent values), even for distances far away from the graphene sheets where the average τ_{seg} is similar to its bulk value.

(c) *Translational* segmental dynamics of PE chains was examined through the calculation of the average segmental mean-square displacement. PE chains closest to the graphene layers are slower, compared to the bulk one, for all model PNC systems. In addition, there is a slight dependence of the PE segmental msd on the size of the graphene sheet mainly in the short time (~5–20 ps) regime, *i.e.*, the smaller the sheet the larger the PE atoms msds. Equilibrium desorption kinetics of polymer atoms and chains' center of masses that are initial close to the graphene sheet, was also found to follow a rather broad distribution of characteristic times, which is an additional indication of the strong dynamic heterogeneities induced in the PNCs due to the polymer/graphene interfaces.

(d) Moreover, a detailed investigation of the *properties of graphene* sheets in the PNC has been performed. All graphene sheets exhibit a considerable translational motion for the time period of the current simulations (50–100 ns); center-of-mass msds are much larger than their size. As expected the smaller the graphene sheet the higher its mobility. However, a rather long anomalous diffusion regime

has been observed for all systems; *i.e.*, a clear linear regime cannot be found in the time window of the present simulations. Orientational dynamics was also observed for all graphene sheets by following the time evolution of a vector connecting the center of the graphene sheet with a corner atom. For the smallest sheet (S1) orientational relaxation time is about one order of magnitude smaller than the other two systems, whereas the largest sheet (S3) has almost double the relaxation time compared to the S2 system. Finally, fluctuations (wrinkling) of graphene sheets were analyzed. A "wavy" motion is observed with crests and troughs for all systems studied here. In addition, increasing amplitude of fluctuations is observed as the size of the graphene sheets become bigger.

Overall, due to the importance of heterogeneities discussed above computation of the full distribution of dynamical properties of polymer/graphene PNCs is required. This has been recently recognized also in other hybrid polymeric systems, such as miscible polymer blends [32]. This will be the subject of a future work. Finally, the dependence of the properties of the PNC on the exact interaction between the polymer matrix and the graphene sheet is a very important issue. Current work concerns the study of functionalized graphene (reduced graphene and graphene oxide) into polar and non-polar polymer matrices.

Supplementary Materials

Supplementary materials can be accessed at http://www.mdpi.com/2073-4360/7/3/0390/s1.

Acknowledgments

Author Contributions

All authors have contributed in all parts of the present work.

Appendix: Atomistic Force Field

Table A1. Model parameters and functional forms of all non-bonded interactions of the atomistic force field used here.

Non-Bonded Interactions			
$V_{LJ}(r_{ij}) = 4\varepsilon_{ij}\left[\left(\dfrac{\sigma_{ij}}{r_{ij}}\right)^{12} - \left(\dfrac{\sigma_{ij}}{r_{ij}}\right)^{6}\right], r \leq R_c$			
Atom Types	**mass (g/mol)**	**σ (nm)**	**ε (kJoule/mol)**
CH_2	14.027	0.395	0.3824
CH_3	15.035	0.395	0.3824
C_{GR}	12.011	0.347	0.2750

Table A2. Model parameters and functional forms of all bonded interactions of the atomistic force field used here.

Bonded Interactions		
$V_b(r_{ij}) = \frac{1}{2} k_{ij}^b (r_{ij} - b_{ij})^2$		

Bond	b (nm)	k^b (kJ/mol·nm²)
CH_2–CH_2	0.154	100,000.00
CH_2–CH_3	0.154	100,000.00
CH_3–CH_2	0.154	100,000.00

$V_{morse}(r_{ij}) = D_{ij} \left[1 - \exp\left(-\beta_{ij}(r_{ij} - b_{ij}) \right) \right]^2$			

Bond	b (nm)	D (KJ·mol⁻¹)	β (nm⁻¹)
C_{GR}–C_{GR}	0.14180	478.90000	21.86700

$V_\alpha(\theta_{ijk}) = \frac{1}{2} k_{ijk}^\theta (\theta_{ijk} - \theta_{ijk}^0)^2$		

Angle	θ° (deg)	k^θ (kJ/mol*rad²)
CH_2–CH_2–CH_2	114	519.611
CH_3–CH_2–CH_2	114	519.611
CH_2–CH_2–CH_3	114	519.611

$V_\alpha(\theta_{ijk}) = \frac{1}{2} k_{ijk}^\theta \left(\cos(\theta_{ijk}) - \cos(\theta_{ijk}^0) \right)^2$		

Angle	θ° (deg)	k^θ (kJ/mol)
C_{GR}–C_{GR}–C_{GR}	120	562.2

$V_{rb}(\varphi_{ijkl}) = \sum_{n=0}^{5} C_n (\cos(\psi))^n$					

Dihedral	C_0 (KJ/mol)	C_1 (KJ/mol)	C_2 (KJ/mol)	C_3 (KJ/mol)	C_4 (KJ/mol)	C_5 (KJ/mol)
CH_3–CH_2–CH_2–CH_2	9.2759	12.1545	−13.1168	−3.0585	26.2378	−31.4929
CH_2–CH_2–CH_2–CH_2	9.2759	12.1545	−13.1168	−3.0585	26.2378	−31.4929
CH_2–CH_2–CH_2–CH_3	9.2759	12.1545	−13.1168	−3.0585	26.2378	−31.4929
C_{GR}–C_{GR}–C_{GR}–C_{GR}	25.1200	0.0000	−25.1200	0.0000	0.0000	0.0000

Conflicts of Interest

The authors declare no conflict of interest.

References

1. Lv, C.; Xue, Q.; Xia, D.; Ma, M.; Xie, J.; Chen, H. Effect of Chemisorption on the Interfacial Bonding Characteristics of Graphene Polymer Composites. *J. Phys. Chem. C* **2010**, *114*, 6588–6594.
2. Novoselov, K.S.; Geim, A.K.; Morozov, S.V.; Jing, D.; Zhang, Y; Dubonos, S.V.; Grigorieva I.V.; Firsov, A.A. Electric field effect in atomically thin carbon films. *Science* **2004**, *306*, 666–669.
3. Kim, H.; Abdala, A.A.; Macosko, C.W. Graphene/polymer nanocomposites. *Macromolecules* **2010**, *43*, 6515–6530.
4. Wenrong, Y.; Kyle, R.R.; Simon, P.R.; Pall, T.; Gooding, J.J.; Filip, B. Carbon nanomaterials in biosensors. Should you use nanotubes or graphene? *Angew. Chem. Int. Ed*. **2010**, *49*, 2114–2138.
5. Potts, J.R.; Dreyer, D.R.; Bielawski, C.W.; Ruoff, R.S. Graphene-based polymer nanocomposites. *Polymer* **2011**, *52*, 5–25.

6. Zhang, J.; Jiang, D. Molecular dynamics simulation of mechanical performance of graphene/graphene oxide paper based polymer composites. *Carbon* **2014**, *67*, 784–791.

7. Ramanathan, T.; Abdala, A.A.; Stankovich, S.; Dikin, D.A.; Herrera-Alonso, M.; Piner, R.D.; Adamson, D.H.; Schniepp, H.C.; Chen, X.; Ruoff, R.S.; *et al*. Functionalized graphene sheets for polymer nanocomposites. *Nat. Nanotechnol.* **2008**, *3*, 327–331.

8. Cai, D.; Song, M. Recent advance in functionalized graphene/polymer nanocomposites. *J. Mater. Chem.* **2010**, *20*, 7906–7915.

9. Hentschke, R.; Winkler, R.G. Molecular dynamics simulation study of the adsorption of chain alkanes from solution onto graphite. *J. Chem. Phys.* **1993**, *99*, 5528–5534.

10. Yang, J.S.; Yang, C.L.; Wang, M.S.; Chen, B.D.; Ma, X.G. Crystallization of alkane melts induced by carbon nanotubes and graphene nanosheets: A molecular dynamics simulation study. *Phys. Chem. Chem. Phys*. **2011**, *13*, 15476–15482.

11. Jang, C.; Nouranian, S.; Lacy, T.E.; Gwaltney, S.R.; Toghiani, H.; Pittman, C.U., Jr. Molecular dynamics simulations of oxidized vapor-grown carbon nanofiber surface interactions with vinyl ester resin monomers. *Carbon* **2012**, *50*, 748–760.

12. Nouranian, S.; Jang, C.; Lacy, T.E.; Gwaltney, S.R.; Toghiani, H.; Pittman, C.U., Jr. Molecular dynamics simulations of vinyl ester resin monomer interactions with a pristine vaporgrown carbon nanofiber and their implications for composite interphase formation. *Carbon* **2011**, *49*, 3219–3232.

13. Karatasos, K. Graphene/hyperbranched polymer nanocomposites: Insight from molecular dynamics simulations. *Macromolecules* **2014**, *47*, 8833–8845.

14. Konatham, D.; Bui, K.N.D.; Papavassiliou, D.V.; Striolo, A. Simulation insights into thermally conductive graphene-based nanocomposites. *Mol. Phys.* **2011**, *109*, 97–111.

15. Skountzos, E.N.; Anastassiou, A.; Mavrantzas, V.G.; Theodorou, D.N. Determination of the mechanical properties of a poly(methyl methacrylate) nanocomposite with functionalized graphene sheets through detailed atomistic simulations. *Macromolecules* **2014**, *47*, 8072–8088.

16. Montazeri, A.; Rafii-Tabar, H. Multiscale modeling of graphene-and nanotube-based reinforced polymer nanocomposites. *Phys. Lett. A* **2011**, *375*, 4034–4040.

17. Harmandaris, V.A.; Daoulas, K.C.; Mavrantzas, V.G. Detailed atomistic simulation of a polymer melt/solid interface: Structure, density and conformation of a thin polyethylene melt film adsorbed on graphite. *Macromolecules* **2005**, *38*, 5780–5795.

18. Rissanou, A.N.; Harmandaris, V. Dynamics of various polymer-graphene interfacial systems through atomistic molecular dynamics simulations. *Soft Matter* **2014**, *10*, 2876–2888.

19. Bellido, E.P.; Seminario, J.M. Molecular dynamics simulations of folding of supported graphene. *J. Phys. Chem. C* **2010**, *114*, 22472–22477.

20. Rissanou, A.N.; Harmandaris, V. Structure and dynamics of poly(methyl methacrylate)/graphene systems through atomistic molecular dynamics simulations. *J. Nanopart Res.* **2013**, *15*, 1–14.

21. Rissanou, A.N.; Harmandaris, V. A Molecular dynamics study of polymer/graphene nanocomposites. *Macromol. Symp.* **2013**, *331–332*, 43–49.

22. Martin, M.G.; Siepmann, J.I. Transferable potentials for phase equilibria. 1. United-atom description of *n*-alkanes. *J. Phys. Chem. B* **1998**, *102*, 2569–2577.

23. Walther, J.H.; Jaffe, R.; Halicioglu, T.; Koumoutsakos, P. Carbon nanotubes in water: Structural characteristics and energetics. *J. Phys. Chem. B* **2001**, *105*, 9980–9987.

24. Hess, B.; Kutzner, C.; van der Spoel, D.; Lindahl, E. GROMACS 4: Algorithms for highly efficient, load-balanced, and scalable molecular simulation. *J. Chem. Theory Comput.* **2008**, *4*, 435–447.

25. Berendsen, H.; van der Spoel, D.; van Drunen, R. GROMACS: A message-passing parallel molecular dynamics implementation. *Comput. Phys. Commun.* **1995**, *91*, 43–56.

26. Rissanou, A.N.; Harmandaris, V. Structural and dynamical properties of polystyrene thin films supported by multiple graphene layers. *Macromolecules* **2014**, submitted for publication.

27. Kotelyanskii, M.; Theodorou, D.N. *Simulation Methods for Polymers*; Marcel Dekker Inc.: New York, NY, USA, 2004.

28. Turzi, S.S. On the Cartesian definition of orientational order parameters. *J. Math. Phys.* **2011**, *52*, 053517:1–053517:29.

29. Williams, G.; Watts, D.C. Non-symmetrical dielectric relaxation behaviour arising from a simple empirical decay function. *Trans. Faraday Soc.* **1970**, *66*, 80–85.

30. Meyer, J.C.; Geim, A.K.; Katsnelson, M.I.; Novoselov, K.S.; Booth T.J.; Roth S. The structure of suspended graphene sheets. *Nature* **2007**, *446*, 60–63.

31. Fasolino, A.; Los, J.H.; Katsnelson, M.I. Intrinsic ripples in graphene. *Nat. Mater.* **2007**, *6*, 858–861.

32. Harmandaris, V.; Doxastakis M, Molecular dynamics of polyisoprene/polystyrene oligomer blends: The role of self-concentration and fluctuations on blend dynamics. *J. Chem. Phys.*, **2013**, 139, 034904.